COBEM 2023 27TH INTERNATIONAL CONGRESS OF MECHANICAL ENGENEERING

ABCM Brazilian Society of Mechanical Sciences and Engineering
27th ABCM International Congress of Mechanical Engineering
December 04-08, 2023, Florianópolis-SC, Brazil

COB-2023-1927
Validation of Inviscid CFD Analysis for the Generic Future Fighter

Daniel Oliveira Ferreira
Adson Agrico de Paula
Instituto Tecnológico de Aeronáutica, São José dos Campos, SP, 12228-900, Brazil
daanieel01@gmail.com
adson@ita.br
Ney Rafael Sêcco
Instituto Tecnológico de Aeronáutica, São José dos Campos, SP, 12228-900, Brazil
ney@ita.br
Ricardo Galdino da Silva
Instituto de Aeronáutica e Espaço, São José dos Campos, SP, 12228-904, Brazil
ri_galdino@yahoo.com.br

Abstract. *This work presents a numerical investigation of the aerodynamic characteristics for Generic Future Fighter (GFF) subscale model developed initially by Linköping University and evaluated in follow up by collaboration with Instituto Tecnológico de Aeronáutica (ITA). The aerodynamic investigation reflects fighter requirements driven by stealth capabilities, super-cruise and long range presenting moderated swept wing, canard, and V-tail configurations.The main objective of the study is to validate non-viscous numerical results by lift data at subsonic conditions, comparing them with numerical and experimental results, carried-out at ITA wind tunnel test facilities in the Reynolds number condition of 400,000. Moreover, an extensive evaluation of the flow topology was performed in order to identify main issues of the aerodynamic design. In this sense, validating and evaluating the results bring a non-viscous approach for the use of high-fidelity tools on conceptual design early phase of fighter. Adopting inviscid approach can offer several advantages, including reduced time consumption, enabling a more comprehensive exploration of design during the design phase, and increased cost-efficiency due to diminished computational resource demands, thereby conserving funds for subsequent project stages. The numerical results indicate fidelity compared to viscous analysis and for the experimental lift results.*

Keywords: *CFD, Inviscid Flow, Euler Method, Finite Volume Method, Aerodynamics*

1. INTRODUCTION

In the aircraft design process, the conceptual design phase drives strongly the final design (Buckner *et al.*, 1974), (Raymer, 2006). In this sense, recently, substantial effort has been allocated towards the early stages of combat fighter projects, emphasizing the importance of developing a well-established initial framework that allows a more precise and rapid design (Liangliang *et al*. (2016), Sepulveda and Smith (2019)).

De Resende (2004) describes the evolution of the methodologies used for tools in aerodynamic analysis at Embraer. The author reveals the improvement in fidelity of the aerodynamic tools on design from panel methods for two-dimensional analyses to three-dimensional Computational Fluid Dynamics (CFD) simulations based on the Navier-Stokes equations. As one of these methodologies, non-viscous simulation in CFD appears as appropriated tool for the conceptual design of a combat fighter due to the inviscid nature of the flow phenomena of a delta wing (Anderson, 2017). Exploring the approach of this numerical method, numerous studies have been conducted to validate the efficacy of a non-viscous solution as an appropriate preliminary analysis.

Reddy and Mahesh (2019) conclude that for conceptual design phase, an unstructured Euler based CFD appears to be the best method when compared to experimental data. This numerical method also allows non-expert users generate quickly a mesh for complex geometry and provide rapid results for the flow field without the need for a boundary layer or turbulence model. However, due to the absence of interaction between the boundary layer and shock wave, the results produced a discrepancy with the validation. Todd (1998) and Finley (1995) demonstrated the success in the applicability of Euler-based CFD in a study of different combat fighter configurations. The flow phenomena for fighter wing present several non-linearities such as shock waves, vortical structures, and separated flow. Even so, the data reveal that up to 15° of angle of attack (AoA), the inviscid results were quite accurate. However, in the case of larger angles, they presented less accuracy. When compared with the data from a Navier-Stokes simulation, the results present suitable fidelity for tools at early phases of aircraft design, except for the geometry with the deflected flap, where the boundary layer detachment was fundamental for Navier-Stokes to surpass the Euler method. Both studies also demonstrated the accuracy of the method in lateral-directional data. Moreover, Kinard *et al.* (1996) compared two fighter configurations under two distinct conditions, Mach 0.4 and 0.85. In the subsonic condition, the focus of the present study, the pressure coefficient peak of the vortex was over predicted at all angles, but the compressibility increments were well predicted. A Navier-Stokes solution should

be employed in order to achieve more accurate results. However, Kinard *et al.* (1995), Newsome and Thomas (1985), Newsome (1986) and Raj and Long (1985) describe the problems of employing an non-viscous solution in such vortex-dominated flows: the method successfully captures the overall features of vortex flows including vortex burst but fails to adequately model many of the details such as secondary separated flow, and care must be taken in applying Euler as the solutions exhibit sensitivity to grid density. Nevertheless, in the authors' view, even with the deficiency in capturing these secondary phenomena, with proper caution regarding artificial vorticity production and numerical dissipation, the results from Euler simulations can be employed in initial design stages.

In terms of vortex breakdown studies, Kumar (1998) shows good agreement between inviscid results and Navier-Stokes method. The latter, however, showed better results in breakdown location in cases where the breakdown approached the wing apex. Agrawal *et al.* (1992) also corroborates the applicability of Euler solutions in measuring the breakdown process.

The objective of the present study is to validate the applicability of an inviscid solution as a design tool in the conceptual phase for fighter design by conducting numerical simulations for the Generic Future Fighter (GFF) and comparing lift results with experimental data. In addition, a qualitative analysis of the flow topology is performed in order to clarify the aerodynamic characteristics observed on GGF design dominated by the leading edge vortex.

2. GFF MODEL

2.1 Geometry

The GFF was a design exercise conducted by various Swedish organizations between 2006 and 2009. This aircraft has been utilized by Linköping University, the Instituto Tecnológico de Aeronáutica (ITA), and the University of São Paulo (USP) for novel technological advancements and research (Lundström *et al.*, 2016), (Nepomuceno *et al.*, 2022). Figure 1 depicted the overall layout configuration including V-tail and a canard. The simulated aircraft represents a 3.25% scale model. Table 1 shows relevant geometric characteristics of the model.

Table 1: Wing geometric description

Aspect Ratio	**Taper Ratio**	**Area** [m^2]	**Leading-edge Sweep** [°]	**MAC** [m]
2.35	0.16	0.057	46.90	0.157

Figure 1: GFF model to be simulated (without landing gear)

2.2 Data

The data available for comparison comes from Nepomuceno (2022), which is a C_L curve for angles of attack up to 35° derived from a wind tunnel campaign at a Reynolds number of 400,000. Additionally, data from a viscous CFD simulation (Jouannet *et al.*, 2017) were also used in order to compare the inviscid and viscous results, considering that the article showed a good correlation between the experimental data and the presented results. The wind tunnel tests took place at the ITA facility. It is an open-circuit wind tunnel with a test section 1 m high, 1.28 m wide (average), and 4 m long. Its maximum speed is 80 m/s with a corresponding Mach number of 0.23.

3. COMPUTATIONAL METHODOLOGY

3.1 Flow Solver

The simulations are performed with the CFD++ commercial package (Metacomp Technologies Inc., 2023). CFD++ is an unstructured finite volume flow solver applicable to arbitrary cell topologies including prisms, tetrahedra, hexahedral and polyhedral. It has the capability of solving the full Navier-Stokes equations with high-order spatial and temporal accuracy. To resolve the inviscid Euler equations, the solver uses a pseudo time marching approach where the initial condition is integrated over time until convergence is reached. The convergence can be accelerated by using spatially varying time steps. The three governing equations, mass, momentum and energy conservation, are described in Eq. 1, 2 and 3 respectively.

$$\frac{\partial \rho}{\partial t} + \nabla \cdot (\rho \mathbf{u}) = S \tag{1}$$

$$\frac{\partial (\rho \mathbf{u})}{\partial t} + \nabla \cdot (\rho \mathbf{u}\mathbf{u} + p\mathbf{I}) = S \tag{2}$$

$$\frac{\partial E}{\partial t} + \nabla \cdot ((E + p)\mathbf{u}) = S \tag{3}$$

In the present study, CFD++ was run with a second order spatial discretization scheme. The inviscid fluxes were calculated based on the minmod TVD limiter. The fluxes on the cell faces were reconstructed based on nodal polynomials. The time step sizes were based on the local CFL (Courant Friedrichs-Lewy) number, ramping from 1 to 100 in the first 200 iterations. From the 200th to the 300th iteration, a spatial scheme blending approach was employed to foster numerical stability, blending from first to second order within this interval. The boundary conditions adopted for the simulation comprised a free-stream velocity of 38.02 m/s, air density of 1.225 kg/m^3 and air temperature of 15°C and slip walls for the aircraft surface.

Lastly, the alpha sweep technique was adopted to guarantee that each subsequent angle would commence with a prior solution, thus providing a beneficial impact on numerical stability and the reduction of residuals.

3.2 Mesh

Three grids were generated in order to conduct a mesh independence study, with 6, 8, and 10 million elements. The observed variation in C_{Lmax} was 3.2% between the coarsest and the finest mesh; therefore, the finest mesh was chosen considering the computational resources limitations available. In future work, with expanded computational capabilities, more refined meshes will be used. The mesh used in this case is presented in Table 2, where the number of surface elements, volumetric elements, and the total can be verified; this mesh composed of tetrahedrons exclusively. The domain was made large enough to allow full flow development with minimal boundary interference.

Table 2: Finest mesh details for the GFF model

Surface Elements	Volumetric Elements	Total
416,242	10,346,917	10,763,159

Figure 2 shows the surface mesh and Fig. 3 which illustrates the volumetric mesh. It has a maximum leading edge size of 0.3mm for the wing and 0.08mm for tail and canard leading edge. In terms of mesh refinement, the leading and trailing edges of all lifting surfaces were carefully refined in order to preserve the curvature of these areas, as well as their respective junctions with the fuselage. The maximum aspect ratio is 16.24, and minimum orthogonality is 0.24. The results were obtained once the solution approximated a steady state or, for higher angles of attack, it achieved a periodic oscillation that was accounted for a sufficient duration to allow a proper average.

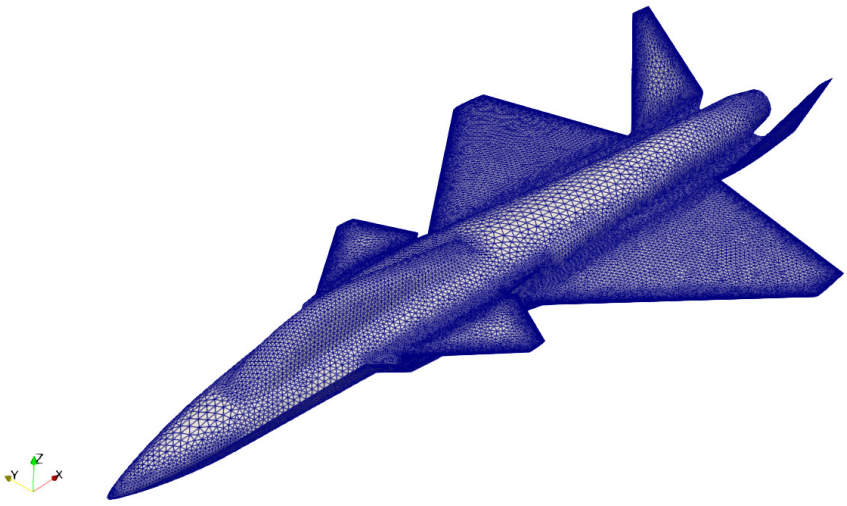

Figure 2: Computational mesh on aircraft surface

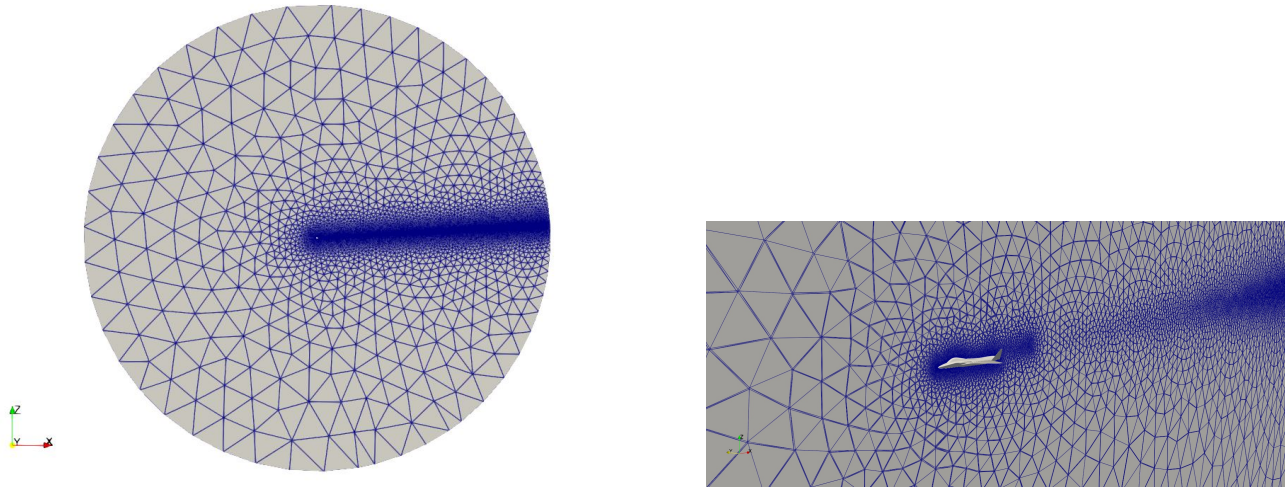

(a) (b)

Figure 3: Computational mesh on domain: a) Far field; b) Near the aircraft

4. RESULTS

4.1 Validation Data

Figure 4 presents numerical and experimental lift curves that support the validation of this work. At lower angle of attack ($\alpha < 5°$), the results indicate the same lift curve slope. At higher angles of attack, a non-linear lift behavior for a delta wing is expected (Anderson, 2017). As the angle increases and the derivative changes, there's a disagreement. The experimental results show the change in curve slope around $\alpha = 6.5°$, while the numerical result postpones the start to $\alpha = 8.7°$. After their respective angles of change, the derivative of the present study increases about 3 times more than that of experimental data, indicating that the wing vortex may have been modeled with greater intensity than the actual one. Table 3 presents the aerodynamic data previously discussed. The parameter α^* stands for the AoA in which the lift slope changes.

As for the effect of vortex breakdown on lift, some researches have reported that for non-slender delta wings, the vortex presents some differences when compared with slender ones and the most relevant for the current study is that the lift force can continue to increase even after vortex breakdown (Earnshaw and Lawford, 1964), (Wentz and Kohlman, 1971). Both viscous and non-viscous curves begin to decrease the lift derivative at $\alpha = 21°$ (an indication of vortex breakdown), while experimental data indicates to $\alpha = 23°$. The C_{Lmax} found in this study was 1.34, while the experimental value was 1.39, indicating a reasonable correlation for the entire C_L curve.

In order to be comparable the current drag results with data from Jouannet *et al.* (2017), the friction drag component

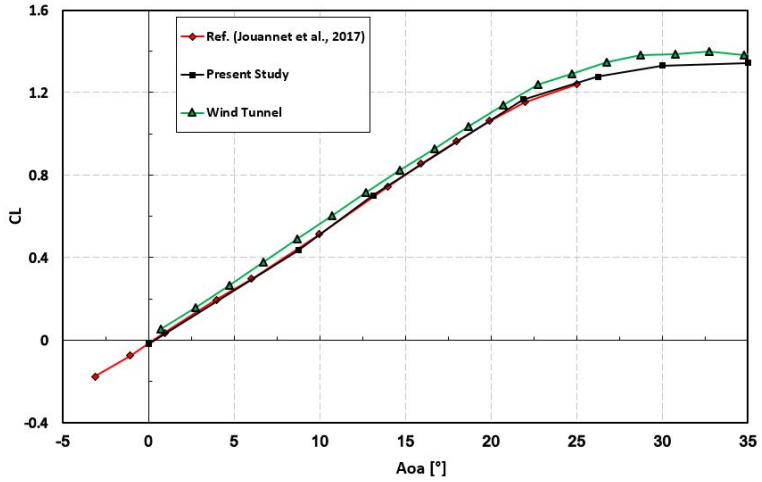

Figure 4: C_L *versus* α comparison

Table 3: Lift curve parameters

Parameter	**Experimental Data (Nepomuceno, 2022)**	**Current Study**
C_{L0}	0.0145	-0.0183
α^* [°]	6.5	8.7
$\partial C_L/\partial\alpha$ for α<α^*	3.11	2.98
$\partial C_L/\partial\alpha$ for α<α^*	3.27	3.48
Increment in $\partial C_L/\partial\alpha$	5.34%	17.16%

due to viscosity did was added, based on a flat plate skin-friction coefficient and typical form factor (Raymer, 2006). At low angle of attack, although the current simulation presents few points, the results indicate a good agreement. Moreover, at high angles of attach (α > 20), the non-viscous simulation even with additional friction drag component underestimates the drag coefficient, indicating that potentially the pressure drag component due to flow separation has not been properly accounted. In according with this non-viscous underestimated drag, Hicks *et al.* (1964) mentioned that the main point of disagreement between the inviscid simulation and experimental data lies at the trailing edge, which has its effect amplified at high angles where vortex breakdown begins to occur.

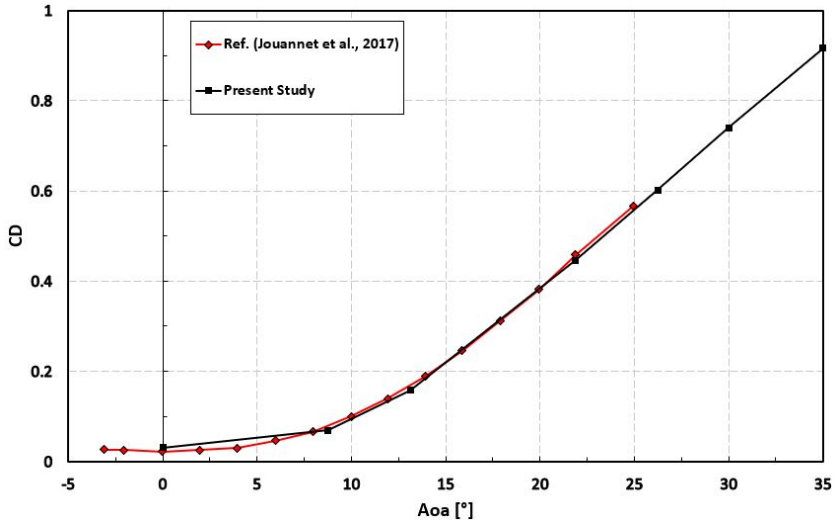

Figure 5: C_D *versus* α comparison

Regarding the C_M data, Jouannet *et al.* (2017) calculates that the neutral point would be 1253 mm from the aircraft nose, which in the scale of the current model would be 313mm. The value found in the present simulation was 300 mm, also from the nose, which corresponds to a difference of 8.9% of the MAC.

4.2 Flow Topology Investigation

Figure 6 presents the pressure distribution on the upper surface of the fighter. The surface pressure distribution indicates the vortical flow over the planform at an AoA of 26° and 35°. Three vortex pressure footprints can be identified: one from the wing, one from the canard, and one that emerges from the chine where it approaches the engine air intake. As the AoA increases, it can be seen that the low pressure zone of the vortex moves away from the surface, whereas at 35°, the angle of C_{Lmax}, it can scarcely be observed over the wing. This indicates the vortex breakdown, as the vortex core is not present as a coherent structure indicated by the aforementioned low pressure zone on surface.

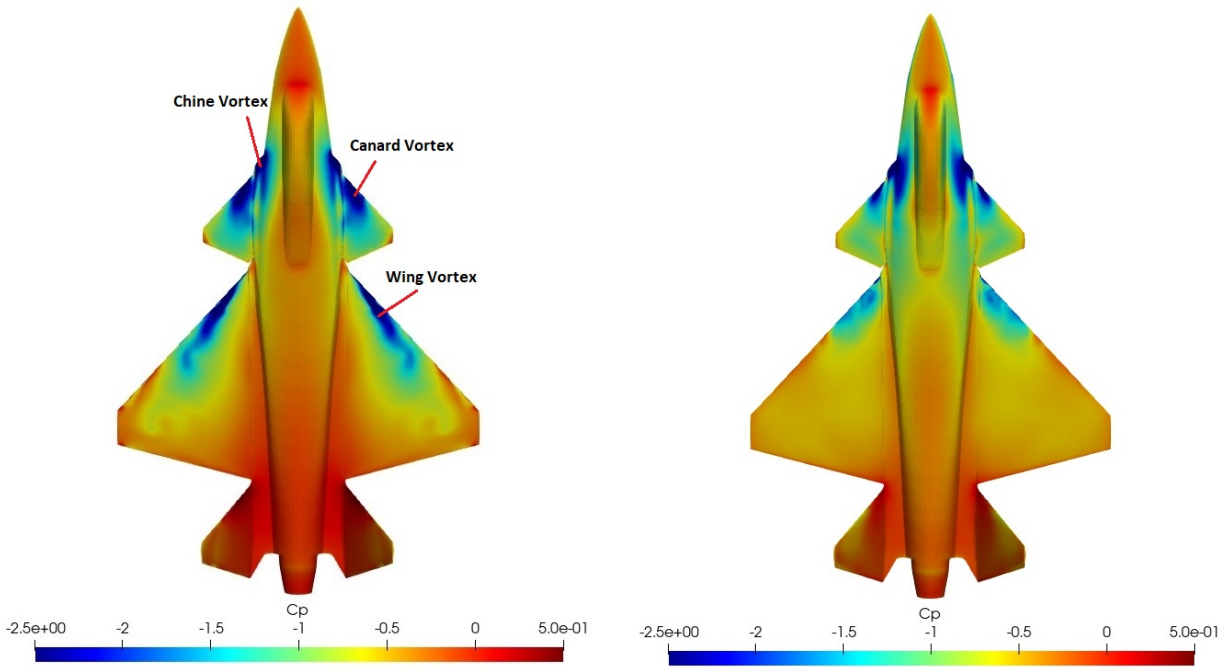

(a) (b)

Figure 6: C_P contourn over the aircraft: a) 26°; b) 35°

For a clear understanding of flow topology, Fig. 7 shows the Q-criterion, a mathematical quantity used to identify coherent structures by highlighting areas where the vorticity magnitude is greater than the magnitude of the rate of strain, colored by axial vorticity, which represents the direction of vortex rotation. Figure 7a has no well-formed vortical structure over the wing and over the canard, except for a vorticity concentrated throughout the junction of the canard with fuselage, originated by the vorticity of the engine air intake. In Fig. 7b, the vorticity at the junction effectively turn into a vortex, whose extension and intensity equate to the canard's vortex itself. At this angle, the two vortices remain separate. On the wing, the vortex begins to form, but the vortex at the wingtip is still dominant. Even though these vortices are weak and do not influence considerably on surface's C_P, their formation from 0° was enough to cause an increase in the derivative of the C_L versus α curve.

Figure 8 shows that the vorticity forming the vortex at the canard-fuselage junction divides into two, in addition to the aforementioned, there is also a part of the vorticity that heads towards the cockpit.. Despite this smaller vortical formation not lasting for a long time, at higher angles it does present a more prolonged alteration in the vorticity field over the fuselage, albeit without much interaction and relevance compared to the other structures. Furthermore, its disappearance indicates a certain numerical dissipation.

One observation can be made regarding the canard-wing vortex interaction. In the studied configuration and for AoA up to 26°, the trajectory of the canard vortex does not interfere with the wing's vortex, as the wing sweep angle is not large enough to bring the vortex near to the apex. Moreover, the presence of the canard induces a downwash velocity field near the trailing edge and an upwash outside of the canard span, which reduces the effective angle of attack at the wing inner section and increases in the outboard region (Soltani *et al.*, 2022), (Davari and Soltani, 2022). This phenomenon can be observed in Fig. 8, where the inner region of the wing has few vortical structures, while at approximately 50% of the wing's span, a large formation occurs in a considerably rapid manner.

To analyze the behavior of the vortices at higher angles of attack more clearly, Fig. 9 shows the difference between the total pressure and atmospheric pressure. This plot is particularly useful since the Q-criterion starts to excessively expand its zone of influence, making the vortices less distinguishable from each other. It can be observed that at approximately half the chord of the canard, there is a fusion between the vortices from the chine and the canard itself; subsequently, they

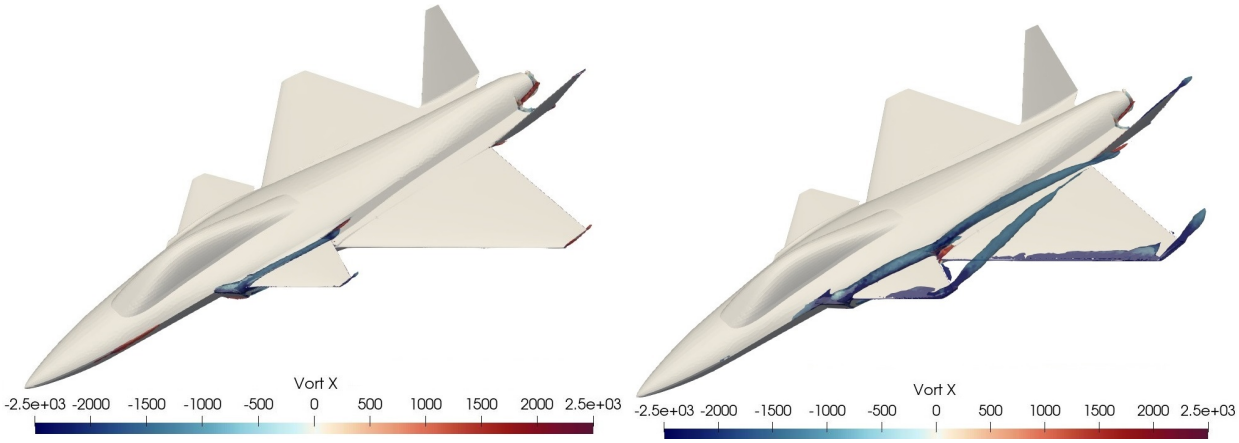

(a) (b)

Figure 7: Q-criterion iso-surface colored by ω_x [1/s] for AoA: a) 0°; b) 8.7°

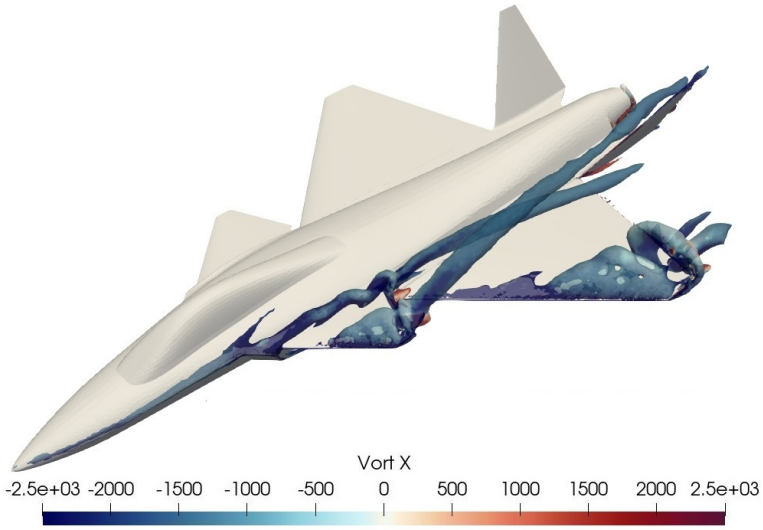

Figure 8: Q-criterion iso-surface colored by ω_x [1/s] for AoA 13°

progress downwind towards the tail. In Fig. 6b, it can be seen the interference of the canard vortex with the tail, marked by the reduction in C_P in the region, which can potentially cause tail buffet effects.

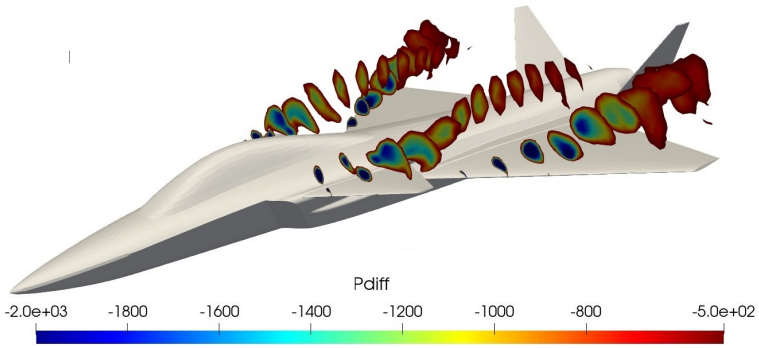

Figure 9: Contour of total pressure minus atmospheric pressure [Pa] for AoA 26°

Approaching the highest simulated AoA, Fig. 10 shows the complete loss of coherence of the vortical structures (vortex breakdown). Both vortices lose their coherent form, marked by a rapid expansion of the vortex core and loss of negative pressure. In the wing vortex, it is observed that it maintains its low-pressure zone cohesive up to around 50% of the root chord for 26°, whereas for 35° it mantains only up to 20%. Moreover, as verified in Fig. 6b, the pressure reduction caused by the vortex over the wing's upper surface ceases to be present just when the vortex breakdown occurs. The canard vortex, on the other hand, manages to stay cohesive up to about 40% of the root chord. A possible explanation for its longer longevity compared to wing vortex is that, as Davari *et al.* (2015) elucidates, the interaction of vortices of

different strengths can amplify the vortex with less strength. Figure 6a and Fig. 6b show that at the beginning of the canard, the chine vortex already has a relevant strenght, which induces a stronger vortex over the canard, making it more resistant to its breakdown.

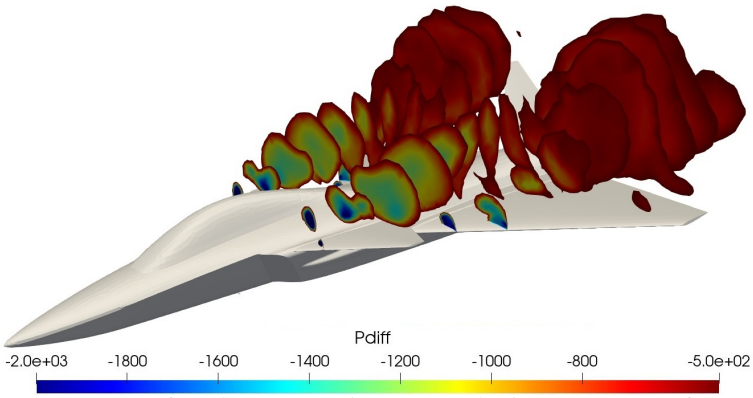

Figure 10: Contour of total pressure minus atmospheric pressure [Pa] for AoA 35°

As previously mentioned, a limitation in the inviscid approach of the leading edge vortex are the secondary structures, characterized by smaller vortice that form between the wing surface and the main vortex, and which have an opposite direction of rotation compared to the main vortex (Anderson, 2017). Figure 11 shows these counter-rotating vortices, which would be defined with a positive vorticity value on the x-axis. However, it is observed that such vortices do not really form into a coherent structure since a significant part of their formation process is the wall viscosity.

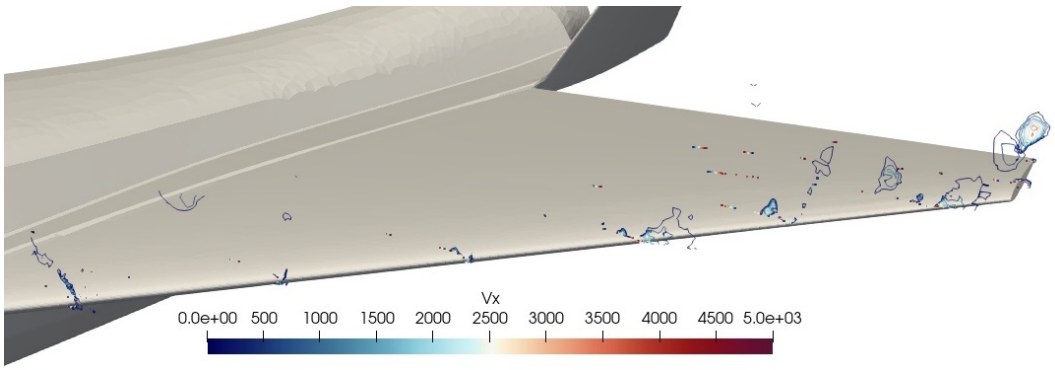

Figure 11: ω_x [1/s] over the wing for AoA 26°

5. CONCLUSIONS

The present study brings primarily the validation of an inviscid model for GFF fighter configuration comparing with experimental. Secondarily, numerical results using Reynolds-Averaged Navier Stokes (RANS) helped to understand the limitation of the non-viscous model. In terms of results, the lift curve indicates underestimated values in entire range of angle of attack. Moreover, the angle of attack at which the non-linearity due to vortex lift began was slightly delayed and the angle of attack at which occurs the onset of substantial loss of lift due to vortex breakdown was slightly advanced. However, the lift results reveal an overall behavior in agreement with wind tunnel data.

The non-viscous drag results corrected with friction drag portion showed the same characteristics with error of 3% in the range of angle of attack. A possible point of disagreement between the data would be the C_D for angles close to C_{Lmax}, requiring more detailed analysis.

Derived from the C_M calculations, there was an advancement in the neutral point position of 8.9% in relation to the MAC based on the numerical data from literature provided.

The flow topology presented in the analysis reveal good agreement with the experimental results from literature indicating good capture of the lift vortex phenomena even limitations of the non-viscous approach such as numerical dissipation present due to mesh size limitation. In addition, the inability of identifying the secondary vortical structures was presented in agreement with other inviscid analyses. Therefore, the present study, within the limitation of the available data, has taken an important step towards the validation of the inviscid solution as a useful tool for using during conceptual design phases of a combat fighter.

6. ACKNOWLEDGEMENTS

The authors would like to acknowledge CAPES for providing a master's scholarship, and Leonardo Nepomuceno for providing the GFF experimental data.

7. REFERENCES

Anderson, J., 2017. *Fundamentals of Aerodynamics*. McGraw-Hill Higher Education, 6th edition.

Buckner, J., Benepe, D. and Hill, P., 1974. "Aerodynamic design evolution of the yf-16". In *Proceedings of the 6th Aircraft Design,Flight Test and Operations Meeting*. Los Angeles, U.S.A.

Davari, A.R., HadiDoolabi, M., Soltani, M.R. and Izadkhah, M., 2015. "Aspects of canard-wing vortices interaction in subsonic flow". *Scientia Iranica*, Vol. 22, pp. 743–754.

Davari, A.R. and Soltani, M.R., 2022. "Impact of canard on the flowfield over the wing in various flow regimes". *AUT Journal of Mechanical Engineering*, Vol. 6, pp. 113–128.

Earnshaw, P.B. and Lawford, J.A., 1964. "Low-speed wind-tunnel experiments on a series of sharp-edged delta wings". In *ARC Reports and Memoranda No 3424*.

Hicks, R.M., Cliff, S.E., Melton, J.E., Langhi, R.G., Goodsell, A.M., Robertson, D.D. and Moyer, S.A., 1964. "Euler and potential experiment/cfd correlations for a transport and two delta-wing configurations". In *NASA Technical Memorandum 102208*.

Jouannet, C., Lundström, D., Krus, P. and Sobron, A., 2017. "Aerodynamic database of a subscale demonstrator". In *Proceedings of the 35th AIAA Applied Aerodynamics Conference*. Denver, U.S.A.

Lundström, D., Sobron, A., Krus, P., Jouannet, C. and da Silva, R.G.A., 2016. "Subscale flight testing of a generic fighter aircraft". In *Proceedings of the 30th Congress of the International Council of the Aeronautical Sciences*. Daejeon, South Korea.

Metacomp Technologies Inc., C., 2023. "MLA works cited: Electronic sources (web publications)". http://www.metacomptech.com/. Accessed 01 Jul 2023.

Nepomuceno, L.M., 2022. *Application of Subscale Flight Testing For Nonlinear Longitudinal Aerodynamic Estimates*. Ph.D. thesis, Instituto Tecnológico de Aeronáutica, São José dos Campos, Brazil.

Nepomuceno, L.M., da Silva, R.G.A., Sobron, A., Krus, P. and Lundström, D., 2022. "Estimation of lift characteristics of a subscale fighter using low-cost experimental methods". *Aircraft Engineering and Aerospace Technology*, Vol. 94, pp. 1379–1389.

Raymer, D.P., 2006. *Aircraft design: A conceptual approach*. American Institute of Aeronautics and Astronautics, Reston, Va., 4th edition.

Soltani, M.R., Askari, F., Davari, A.R. and Nayebzadeh, A., 2022. "Effects of canard position on wing surface pressure". *Scientia Iranica*, Vol. 17, pp. 136–145.

Wentz, W.H. and Kohlman, D.L., 1971. "Vortex breakdown on slender sharp-edged wings". *JA Aircraft*, Vol. 8, pp. 156–161.

8. RESPONSIBILITY NOTICE

The authors are solely responsible for the printed material included in this paper.